Two-dimensional dose distribution measurement based on rotational optical fiber array: A Monte Carlo simulation study

Pinyuan Xu [a], Changran Geng [a,b,c,*], Diyun Shu [a], Xiaobin Tang [a,b,c], Huan Liu [a], Feng Tian [a], Huangfeng Ye [a]

[a] Department of Nuclear Science and Technology, Nanjing University of Aeronautics and Astronautics, Nanjing, 210016, China
[b] Joint International Research Laboratory on Advanced Particle Therapy, Nanjing University of Aeronautics and Astronautics, Nanjing, 210016, China
[c] Key Laboratory of Nuclear Technology Application and Radiation Protection in Astronautics(Nanjing University of Aeronautics and Astronautics), Ministry of Industry and Information Technology, Nanjing, 210016, China

ARTICLE INFO

ABSTRACT

Quality assurance is particularly important for modulated radiotherapies which improve dose conformity and involve complex processes of dose delivery. This work proposes a dose measurement method based on a rotational optical fiber array and the Cherenkov effect as an alternative pretreatment quality assurance method. Monte Carlo simulation toolkit Geant4 is used to study the accuracy and influencing factors of this method. Four different shapes of radiation field are designed to explore the influence of different reconstruction algorithms, fiber spacing, rotation angles, and radiation types on the accuracy of dose field measurement. The results show that the difference between the reconstructed dose field and the reference dose field is within 8% under the irradiation of uniform radiation field. To obtain high-precision reconstructed images, the fiber spacing should be within 2 mm, and at least 60 angles of projection data should be acquired when the fiber array is rotated 180°. In conclusion, the proposed new method using a rotating fiber array can reconstruct the radiation field distribution rapidly, and provides accurate information on the shape and intensity distribution of the radiation field. Further studies are needed to improve the accuracy and feasibility in real clinical practice.

1. Introduction

Modulated radiotherapies such as intensity modulated radiation therapy (IMRT) and volume modulated arc therapy are used to produce beams capable of delivering complex dose distributions within a patient, thereby improving the dose conformity and potentially reducing radiation side effects on normal tissues. The planning and the delivery of modulated treatments involve complex processes, which increase the possibilities of inaccuracies in treatment. Therefore it is important to verify the accuracy of the beam data used by the treatment-planning system and test the accuracy with which treatments can be delivered (e.g. pretreatment quality assurance (QA) of patient treatments). Measuring the two-dimensional (2D) dose distribution is one of the most important procedures. At present, the commonly used methods for 2D dose distribution measurement of pretreatment QA in clinical practice include film dosimeters (Rodríguez et al., 2020), matrix ionization chambers (Widodo et al., 2020), electronic portal imaging devices (EPID) (Cheng, 2020), and thermoluminescent dosimeters (Izewska and

Andreo, 2000). These methods have both advantages and disadvantages; for example, the resolution of ion chamber based 2D detectors is often larger than ~2.5 mm, limited by the cavity volume (Markovic et al., 2014). Meanwhile, film dosimeters are disposable and mostly used to measure the cumulative dose distribution off-line. The semiconductor-based detectors (e.g. EPID) always have energy and angular dependencies (Smith et al., 2013; Torres-Xirau et al., 2017). Other techniques, e.g. liquid scintillator, μ-Al2O3: C, and Mg radioluminescence films, etc., have also been proposed for the 2D dose distribution in recent studies (Jenkins et al., 2015; Kane et al., 2016; Markovic et al., 2014; Nascimento et al., 2020; Wong et al., 2012).

Due to small size, low mass, immunity to electromagnetic interference (Villnow et al., 2014), on-line, and remote measurement, optical fibers have some advantages in radiation measurement (O'Keeffe et al., 2015). Optical fiber dosimeters include scintillation fiber dosimeters (Beaulieu and Beddar, 2016), thermoluminescence fiber dosimeters (Sani, 2015), optically stimulated luminescence fiber dosimeters (Kalnins et al., 2012), radioluminescence fiber dosimeters (Darafsheh,
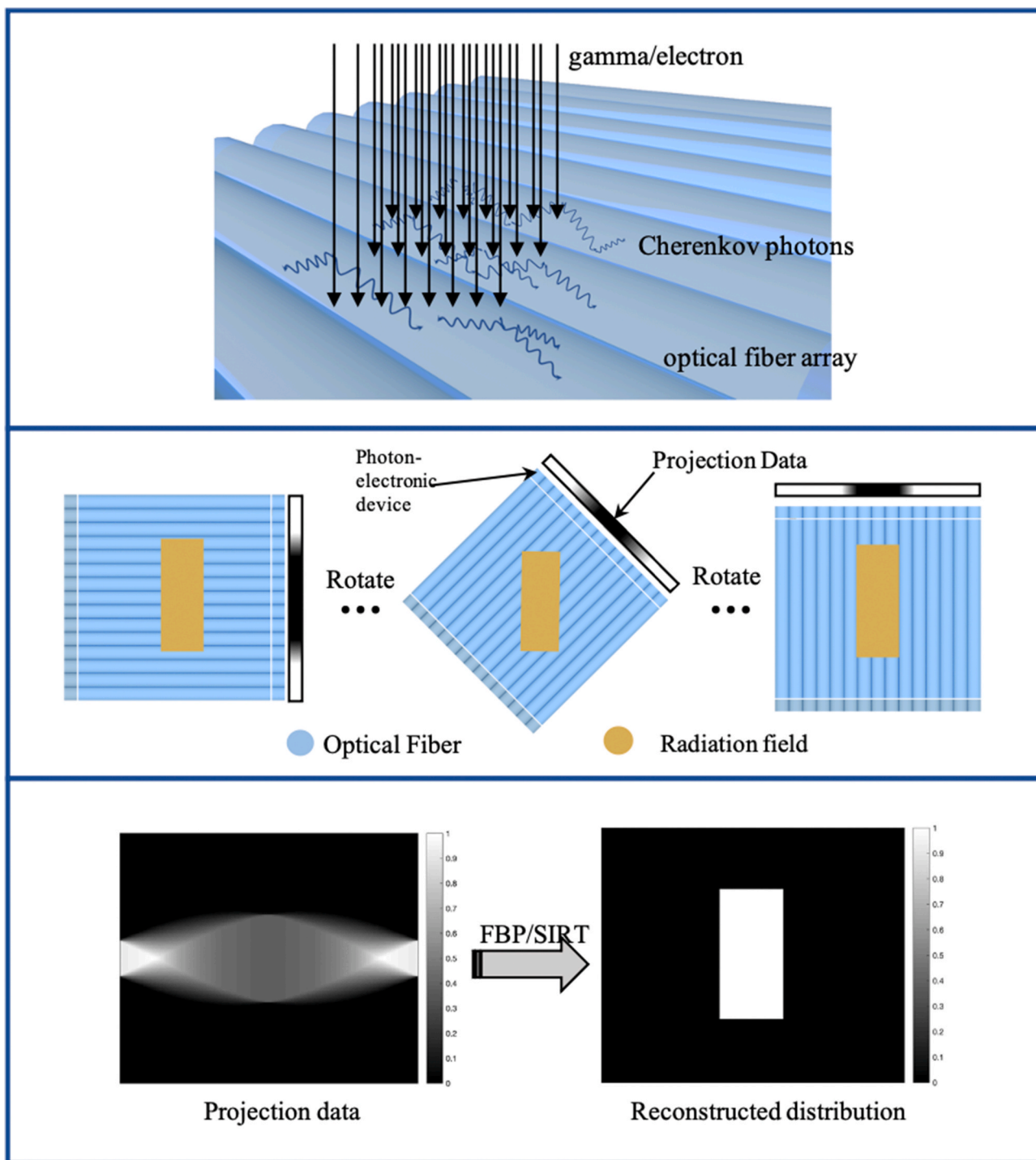

Fig. 1. Principle of dose measurement.

2019), and optical absorption dosimeters (Tomashuk et al., 2014) etc. Using the fiber dosimeters mentioned above, many researchers have placed the fibers into an array to measure multi-point dose deposition or even 2D dose deposition. Archambault et al. (2007) developed a fiber array using scintillation fibers, and compared the difference of dose deposition in the axial and off-axis directions with that measured by ionization chambers. The results show that this kind of optical fiber array is a valuable tool in evaluating dose field distribution. Lee et al. (2008) used a fiber-optic radiation sensor coupled with an organic scintillator to measure the high-energy photon beam from a clinical linear accelerator. The spatial resolution of this sensor was less than 5.0 mm. Goulet et al. (2012) proposed a tomodosimeter using long scintillation fiber arrays to achieve 2D dose measurement. This provides a new method for millimeter-resolution dosimetry on a complete 2D plane using only a few scintillating fibers, which also shows potential for three-dimensional dose distribution measurement (Goulet et al., 2013). Cherenkov photons, as inevitable signal contamination, can be generated inside scintillation fibers which will interfere with reconstruction of the dose field.

Cherenkov radiation can be generated when a charged particle (such as an electron) passes through a dielectric medium at a speed greater than the phase velocity (i.e. speed of propagation of a wave in a
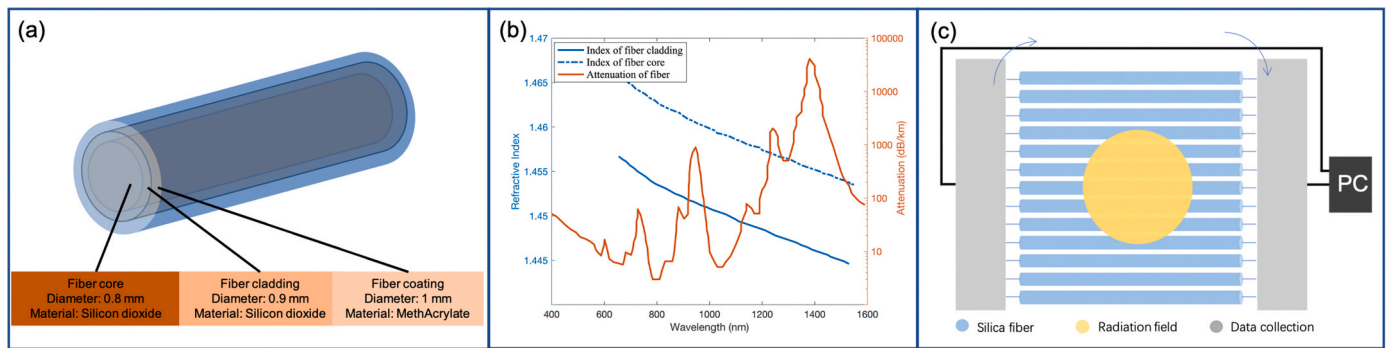
Fig. 2. (a) The structure of optical fiber; (b) properties of optical fiber; and (c) schematic model of optical fiber array.
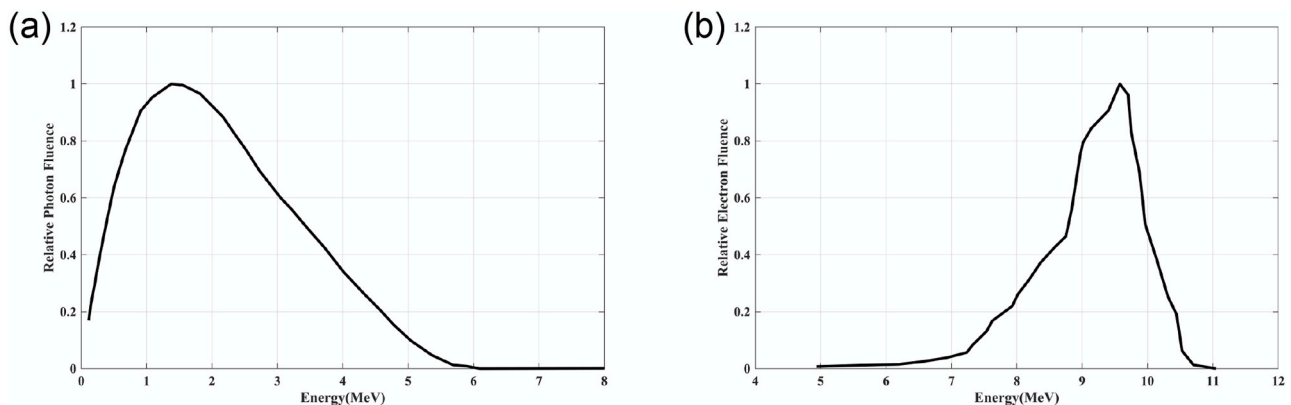

Fig. 3. Energy spectrum of 6 MV photons and 9 MeV electrons: (a) 6 MV photon spectrum and (b) 9 MeV electron spectrum generated by medical linear accelerator.

medium) of light in that medium. Compared with using scintillator photons for radiation dose measuring, using Cherenkov radiation has three advantages: (a) occurs in all dielectric materials, especially some radiation-resistant materials (Brunner and Schaart, 2017; Caravaca et al., 2017), (b) short emission time of about 10^{-9}–10^{-11} s, and (c) no quench effect (Yang et al., 2020). Previous studies (Glaser et al., 2014; Shu et al., 2015; X. Zhang et al., 2018) found that under irradiation of electron or photon beams, the number of photons generated in the fiber show a certain response relationship with the dose deposited in the fiber. However, the Cherenkov radiation is anisotropic, and may affect dose measurement accuracy for absolute measurements.

Combining Cherenkov radiation and rotational fiber array, we describe a 2D dose distribution measurement method providing an alternative method in pretreatment QA. This method has potential advantages of high spatial resolution (about 1 mm) and reusability. A Monte Carlo simulation method is used to study the accuracy and factors influencing of this method. Four different shapes of radiation field are designed to explore the influence of different reconstruction algorithms, fiber spacing, rotation angles, and radiation types on the accuracy of dose field measurement. Finally, a beamlet in IMRT is set to show reconstruction results in a realistic situation.

2. Materials and methods

2.1. Principle of dose measurement based on rotating fiber arrays

The proposed system is composed of a closely arranged fiber array (Fig. 1). When the fibers are irradiated by ionization radiation (e.g. electrons or photons), Cherenkov photons can be generated in each

fiber. The Cherenkov photons are then transported to the end of the fiber and recorded by the photon–electronic devices (e.g. Si-PM). The number of Cherenkov photons generated in the optical fiber is proportional to the energy deposition in that fiber according to previous studies. Therefore the Cherenkov photons are a cumulative measure of the energy deposition in the fiber for a certain situation. Rotating the fiber array allows measurement of the Cherenkov photons generated in each angle of the fiber array. Using the Cherenkov photons in every optical fiber of each angle (i.e. sinogram), the 2D energy deposition distribution can be reconstructed in concept similar to computed tomography (CT). In this work, to simulate the whole process of the method, Geant4.10.05 is used to simulate the process of radiation interaction with matter and also the detailed transportation of Cherenkov photons (Agostinelli et al., 2003; Allison et al., 2006). MATLAB_R2017b is used for reconstruction.

2.2. Configurations of the Monte Carlo simulation

2.2.1. Geometry

The structure of the optical fiber is shown in Fig. 2a. The diameter of optical fiber is set to 1 mm. The diameter is selected for acquiring a relatively high detection efficiency; however, other fibers could be used in the future. The outer dimensions of the coating, cladding, and core of one optical fiber are 1, 0.9, and 0.8 mm according to THORLABS (FT800UMT, THORLABS). The material of the core and cladding is silica dioxide and the coating is polymethyl acetate. The density of the core and cladding is 2.2 g/cm^3 and the density of coating is 0.95 g/cm^3. The optical fibers are closely arranged without spacing. A hundred silica optical fibers with the length of 100 mm are closely arranged into a rectangular array of 100 mm × 100 mm. The distance between the
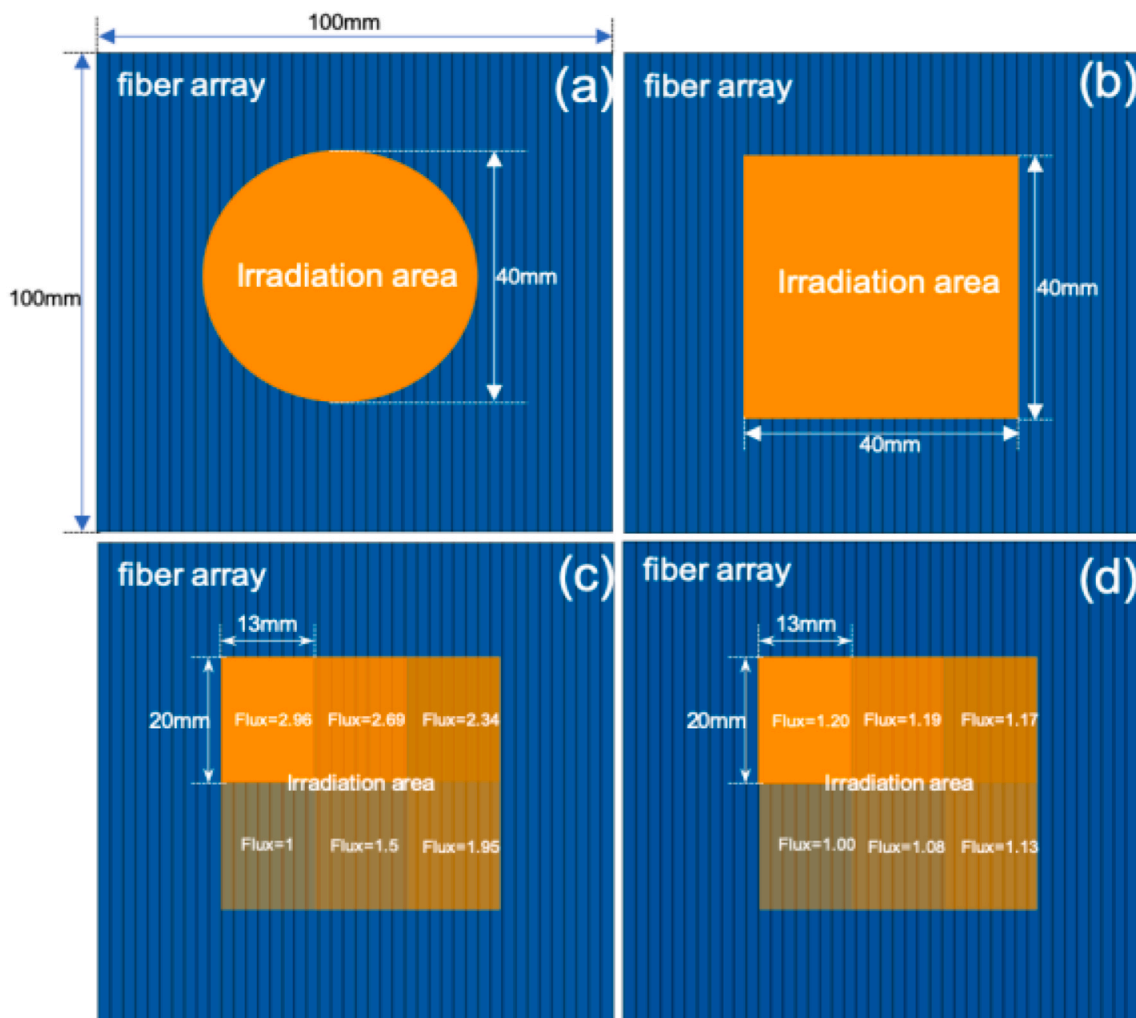
Fig. 4. Radiation source settings in the simulation: (a) circular uniform field with radius 20 mm; (b) square uniform field with size 40 mm × 40 mm; (c) 40 mm × 39 mm square uneven field, the range in degree of unevenness is 10–50%; and (d) 40 mm × 39 mm square uneven field, the range in degree of unevenness is 1–8%.
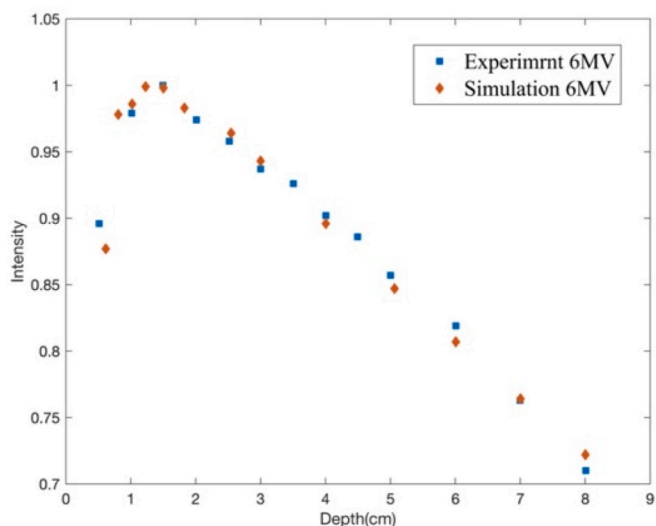

**Fig. 5.** Relative Cherenkov photon yield comparison.

midpoint of two adjacent fiber is 1 mm. Cylindrical detectors are placed at each end of fiber to record the number of optical photons.

2.2.2. Physics list in the simulation

Geant4 is a general-purpose Monte Carlo simulation toolkit for particle transportation and it has been widely used in the field of nuclear technology and application (Allison et al., 2006). In this work, the "standard electromagnetic physics" and "optical physics" processes are applied to simulate the detailed transportation of both ionizing radiations and optical photons. When the charged particles pass through the medium at a speed greater than the phase velocity of the light in the medium, Cherenkov photons will be emitted in the form of a conical wave along the direction of particle motion. The wavelengths of Cherenkov photons in the simulations range within 450–650 nm.

2.2.3. Optical processes in the simulation

In order to simulate the optical processes of Cherenkov radiation inside fiber, it is necessary to take advantage of the optical processes available in Geant4. Taking into account the interaction of optical photons propagating in the fiber, optical properties such as the refractive index, absorption, and scattering of the fiber are added to Geant4 (Anchordoquia et al., 2001). Both refractive index and attenuation are set as a function of wavelength (Fig. 2b). Optical surface is set at the core–cladding and cladding–coating boundaries, ensuring that reflection and refraction occurs. Additionally, Mie scattering and Rayleigh
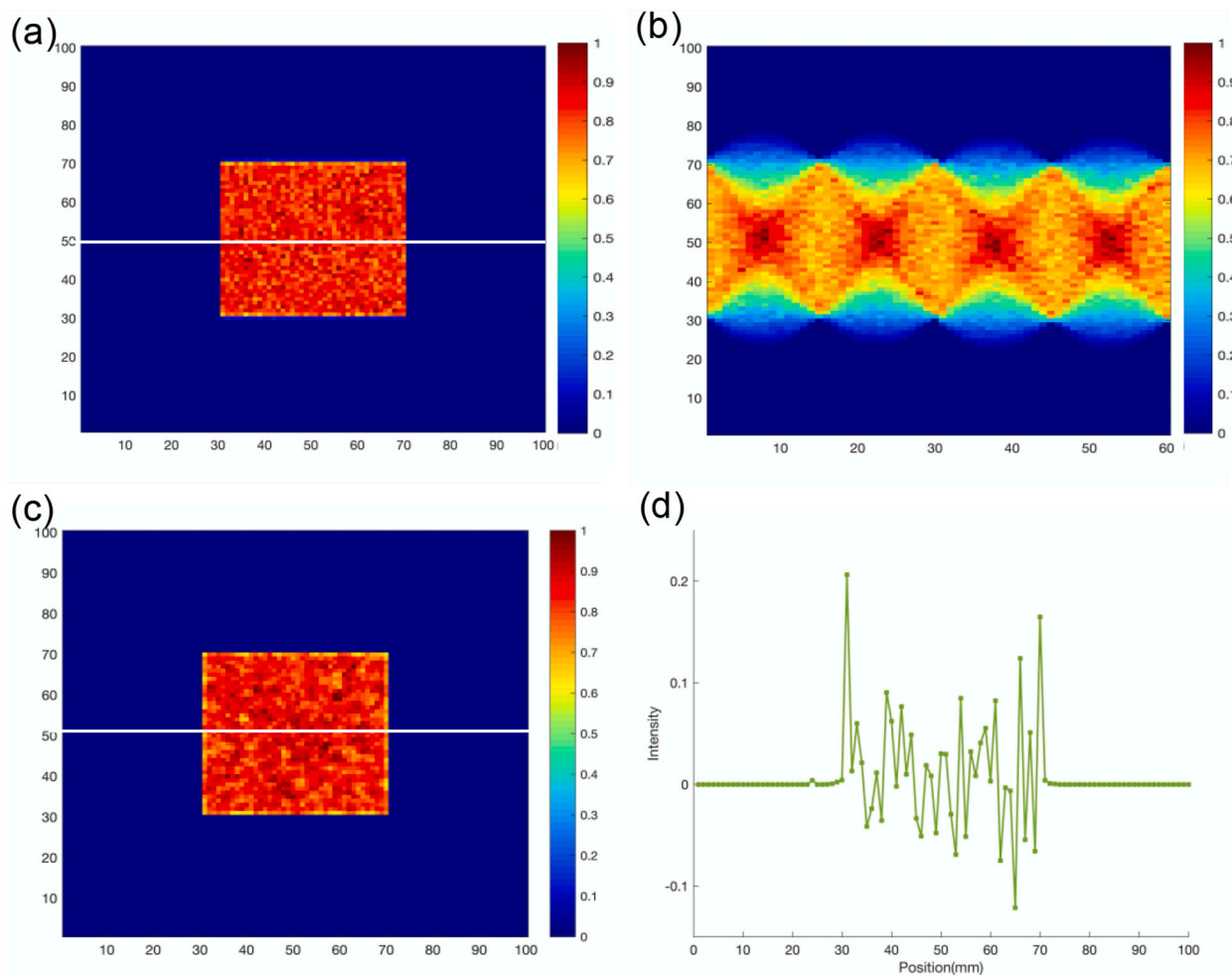
Fig. 6. Reconstruction accuracy comparison of RF1: (a) reference dose distribution of RF1; (b) sinogram of projection data; (c) reconstructed dose distribution of RF1; and (d) difference between reference dose distribution and reconstructed dose distribution.

scattering are available during the propagation of Cherenkov light.

2.2.4. Source definition in the simulation

Four kinds of radiation fields are designed to verify the effectiveness of this method (Fig. 4). For radiation field one (RF1), a circular uniform radiation field is configured with diameter 40 mm (Fig. 4a). For radiation field two (RF2), a square uniform radiation field is set with length 40 mm (Fig. 4b). Two unevenness radiation fields set in the simulation (Fig. 4c and d), which are rectangular radiation fields with size 40 mm × 39 mm consist of six small ones in different flux. For radiation field three (RF3), six different flux distributions are set in a rectangular radiation field, in which the flux ratio in each block is 1, 1.5, 1.95, 2.34, 2.69, and 2.96. Radiation field four (RF4) is similar to RF3 but the flux change is slighter, and the flux ratio in each block is 1, 1.08, 1.13, 1.17, 1.19, and 1.20. In subsequent simulations, the optical fiber array is vertically irradiated by 6 MV photons and 9 MeV electrons. The energy spectrum for them are obtained from published articles (Foster et al., 2014; Patil, 2010) and are shown in Fig. 3.

2.3. Reconstruction algorithm

The most commonly used reconstruction algorithm for medical tomography is the filtered back projection (FBP) technique. This algorithm is derived from the Fourier slice theorem which is achieved by transforming the Fourier transform in polar coordinates and re-determining the limit of integration. In addition, iterative reconstruction techniques, such as algebraic reconstruction techniques and simultaneous iterative reconstruction techniques (SIRT), show better accuracy but with more time required. These iterative reconstruction techniques begin with an assumption value, and compare it to real-time measured values, which are projection data in this work, while making constant adjustments until the two are in agreement. In this work, FBP and SIRT algorithms are used to reconstruct dose distributions for comparison.

2.4. Evaluation factors

The dose distribution in the fiber array calculated by the Monte Carlo simulation is used as the reference to evaluate the accuracy of the method. The reconstructed dose distribution is regarded as the target. Both the reference dose distribution and the target dose distribution are compared after normalizing to the maximum value. Four image quality metrics are applied to validate the reconstructed dose distribution performance, i.e. peak signal-to-noise ratio (PSNR) (Poobathy and Chezian,
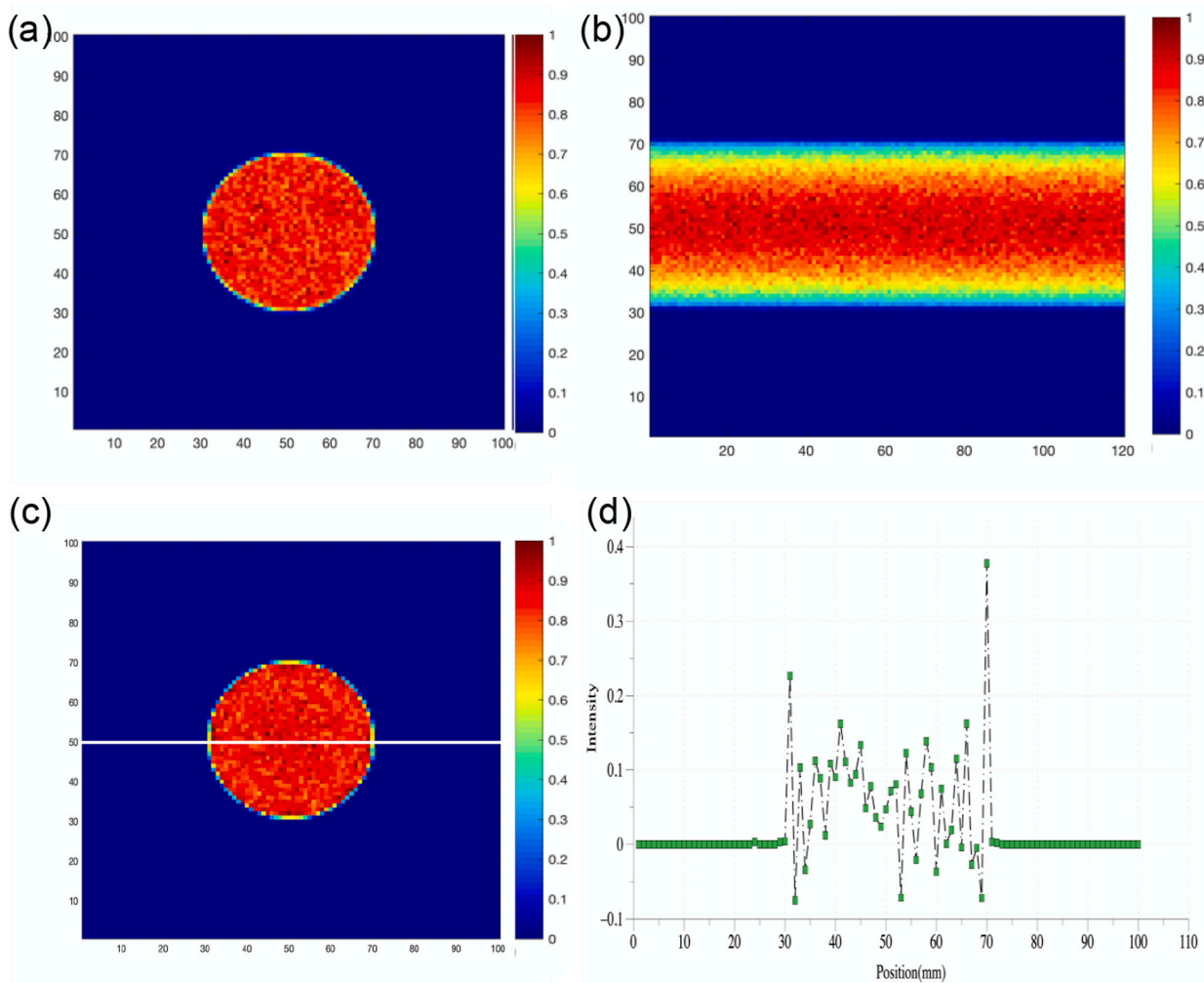
Fig. 7. Reconstruction accuracy comparison of RF2: (a) reference dose distribution of RF2; (b) sinogram of projection data; (c) reconstructed dose distribution of RF2; and (d) difference between reference dose distribution and reconstructed dose distribution.

Table 1
Quantitative comparison of reconstruction effects of different shaped fields.

Radiation Field	PSNR	SSIM	RMSE	VIF
RF1	28.786	0.906	0.036	0.826
RF2	30.494	0.928	0.030	1.009

*RF1, square uniform radiation field; RF2, circular uniform radiation field.

2014), structural similarity (SSIM) (Wang et al., 2004), root mean squared error (RMSE), and visual information fidelity (VIF) (Sheikh and Bovik, 2006). These four metrics measure the image quality from several aspects such as the signal strength (for PNSR), brightness, contrast, structural similarity (for SSIM), error (for RMSE), and information fidelity (for VIF) of the reconstructed image.

3. Results

3.1. Validation of the simulation procedure

Before verifying the effectiveness of this method, we first explore the consistency of relative Cherenkov photon yield at different water depths both in simulation and experimental conditions. A Cherenkov-based optical fiber experiment platform (consisting of the linear accelerator, water-equivalent phantom, optical fiber, single photon counter, and computer) is established. The spectral response range of the single

photon counter (Hamamatsu H11890-210) is 230–720 nm, which can cover the wavelength range of Cherenkov photons. A 6 MV photon beam at 600 MU/min is delivered by the Varian TrueBeam linac. One end of the optical fiber is placed in the center of the radiation field, and the other end is connected with a single photon counter to collect the number of Cherenkov photons generated in the optical fiber under irradiation. The optical fiber is placed under the equivalent water phantom with different thicknesses of 0–8 cm.

The Cherenkov photon yields in different depths of water are shown in Fig. 5. With depth of 0.5–8 cm, the Cherenkov photon yield initially increases and then decreases with the increase in water depth, and the maximum water depth is 1.5 cm. The relative Cherenkov photon yield difference between simulation and experiment is less than 3%, which means the simulation results reflect the actual Cherenkov photon production. At the depth of 0.5 cm, the difference is close to 5% due to the position error during the experiment and the buildup effect. The Cherenkov photon yield measured is about 6.88×10^8 photons per gray, which is potentially strong enough to be detected.

3.2. Uniform dose distribution measurement

Figs. 6 and 7 show two reconstructed uniform dose distributions in different shapes, with reference dose deposition shown in Figs. 6a and 7a. Sinograms composed of the projection data of the dose field at each angle are shown in Figs. 6b and 7b. The rotate step is 3°. Figs. 6c and 7c
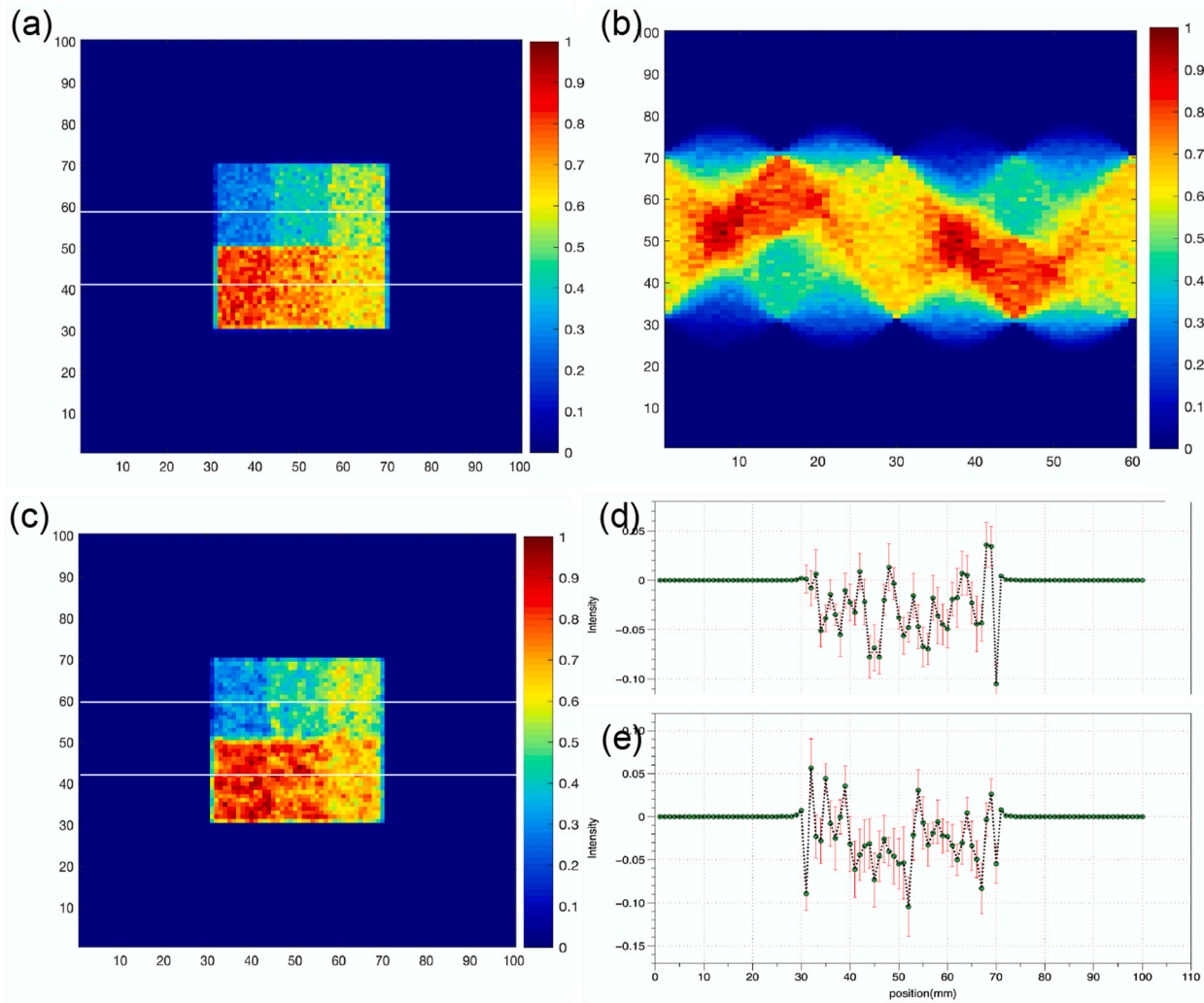
Fig. 8. Reconstruction accuracy comparison of RF3: (a) reference dose distribution of RF3; (b) sinogram of projection data; (c) reconstructed dose distribution of RF3; and (d) difference between reference dose distribution and reconstructed dose distribution.

are the reconstructed dose field distributions based on the SIRT algorithm. Figs. 6d and 7d are the differences between the reference dose distribution and the reconstructed dose distribution; the difference between the centers of the two dose fields is within 8%. Compared to the reference dose distribution, the results show that dose distribution in different shapes can be reconstructed by rotating the fiber array, which shows that the proposed method is potentially feasible.

The reconstruction accuracy of the 2D dose distribution reconstruction is quantitatively shown in Table 1. The results show that in different shapes the measured dose distributions always have high signal-to-noise ratio and low error. The brightness, contrast, structural similarity, and information fidelity of these two results (i.e. two radiation fields) are very close to the reference dose distribution. The VIF of RF2 is close to 1, indicating that there is basically no difference between the reference dose distribution and the reconstructed dose distribution in terms of visual fidelity.

3.3. Dose distribution measurement under non-uniformly distributed radiation field

Figs. 6, 8 and 9 show the dose distribution of squares with three

different uniformities and also show that dose fields with different uniformity levels can be reconstructed generally. Table 2 quantitatively shows the difference between reference dose distribution and reconstructed dose distribution on different uneven radiation fields. The reconstruction results for the two different degrees of inhomogeneity radiation field both have high signal-to-noise ratio, high SSIM, low RMSE, and high information fidelity. Meanwhile, the difference between the reconstructed dose distribution and the reference dose distribution is about 5% in RF3 and RF4.

3.4. Influence of reconstruction algorithm on dose measurement accuracy

Fig. 10 shows the reconstruction of dose distribution under three different radiation fields with different reconstruction algorithms (i.e. FBP and SIRT). In the FBP algorithm, five kinds of filters (Ram-Lak, Shepp-Logan, Cosine, Hamming, and Hann) are used to reconstruct dose distribution. After evaluating the performance of reconstructed images, filter "Shepp-Logan" is selected as the best filter in the FBP algorithm. With streak artifacts existing in the whole image, the FBP algorithm can only roughly show the distribution of the dose field as details are hidden by the artifacts. The iterative reconstruction algorithm can avoid the
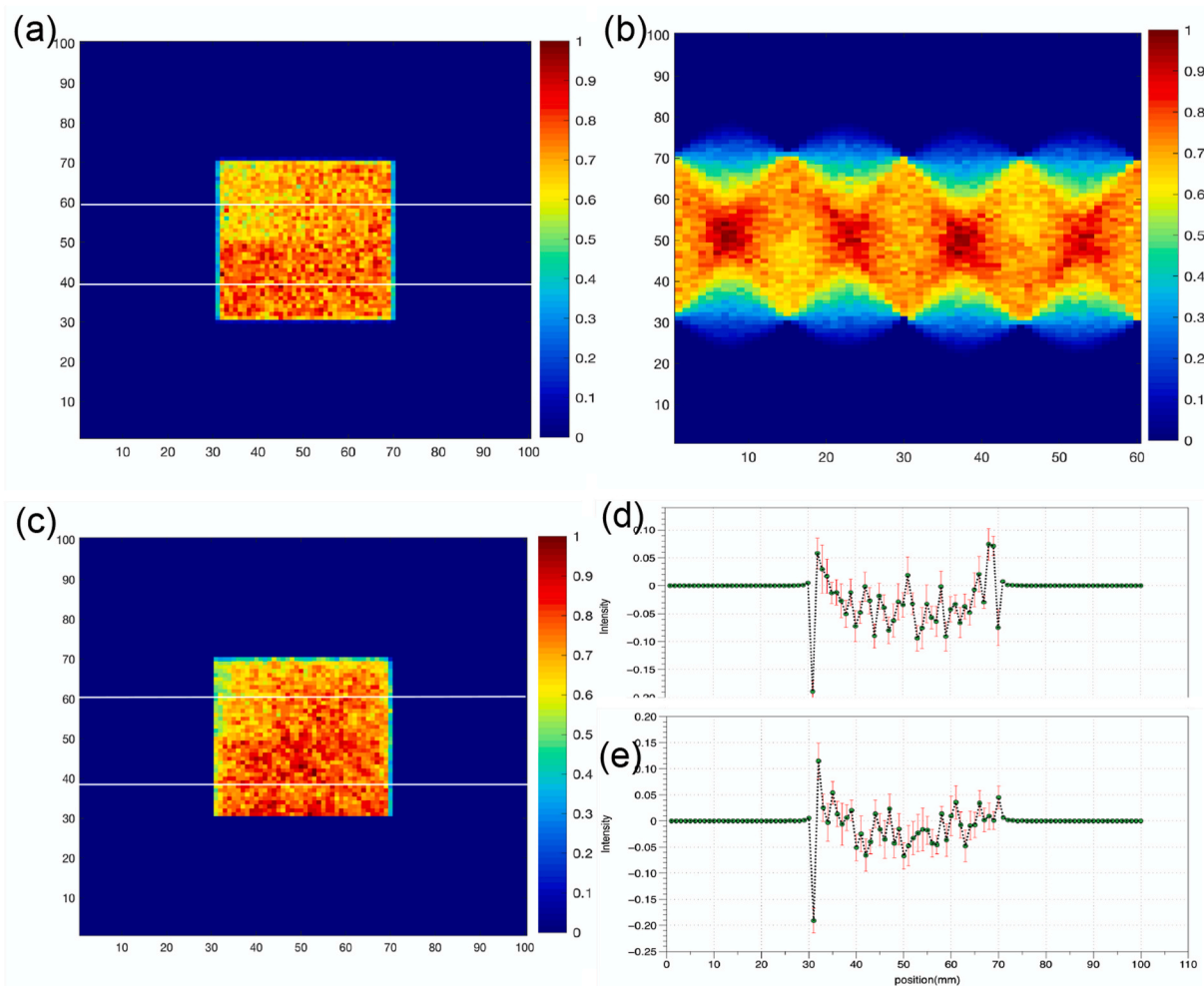
Fig. 9. Reconstruction accuracy comparison of RF4: (a) reference dose distribution of RF4; (b) sinogram of projection data; (c) reconstructed dose distribution of RF4; and (d) difference between reference dose distribution and reconstructed dose distribution.

Table 2
Quantitative comparison of the effect of field reconstruction with different uniformity.

Radiation field[a]	PSNR	SSIM	RMSE	VIF
RF1	28.786	0.906	0.036	0.826
RF3	28.964	0.916	0.036	1.023
RF4	27.177	0.895	0.044	0.944

[a] RF1, square uniform radiation field; RF3, square uneven radiation field, flux ratio 10–50%; RF4, square uneven radiation field, flux ratio 1–8%.

drawbacks caused by the FBP (Fig. 10g–i); in this case, the reconstructed dose distribution has a high similarity compared to the reference. However, in the area where the dose deposition changes sharply, i.e. the edge of the radiation field, the reconstruction result will intuitively have a slight divergence from the reference.

The quantitative results of the influence of different reconstruction algorithms on the dose distribution reconstruction are shown in Table 3. Because these four evaluation factors are used to evaluate the overall image, the striped artifacts in the unirradiated area caused by FBP reconstruction algorithm make it far from an ideal substitute. Comparing the SIRT and FBP algorithms, the use of the FBP algorithm reduces the PSNR by about 42.8%, the RMSE increases by an order of magnitude, and SSIM and VIF also show poor accuracy. The dose distribution obtained using SIRT shows better performance under these four evaluation standards. Therefore, under this measurement standard,

SIRT is better than FBP.

3.5. Influence of fiber spacing on dose measurement accuracy

Fiber spacing is a parameter directly related to the resolution of the dose distribution reconstruction. Understanding the influence of fiber spacing on imaging quality is helpful to improve the accuracy of dose measurement and make an appropriate selection on fiber spacing. Fig. 11 shows the dose field reconstruction result of different fiber spacings in different radiation fields. Fig. 11a–d shows the reconstruction result irradiated by a square uniform field with different fiber spacing. There is an obvious decrease in reconstruction accuracy as fiber spacing increases. The quantified image evaluation factors in the figure also reflect the same phenomenon. Fig. 11e–h and i–l show the reconstruction results of the dose field with different fiber spacings under two kinds of uneven radiation. The reconstruction result decreases as fiber spacing increases, similar to a square uniform radiation field. When the fiber spacing is 1 mm, the difference between the reconstructed dose distribution and the actual dose distribution is about 5%. As the fiber spacing increases to 2 and 4 mm, the difference between the reconstructed dose distribution and the actual dose distribution is about 16% and 27%, respectively. As the radiation field structure becomes more complicated, the distance between the optical fibers must be correspondingly reduced to obtain high-precision results.
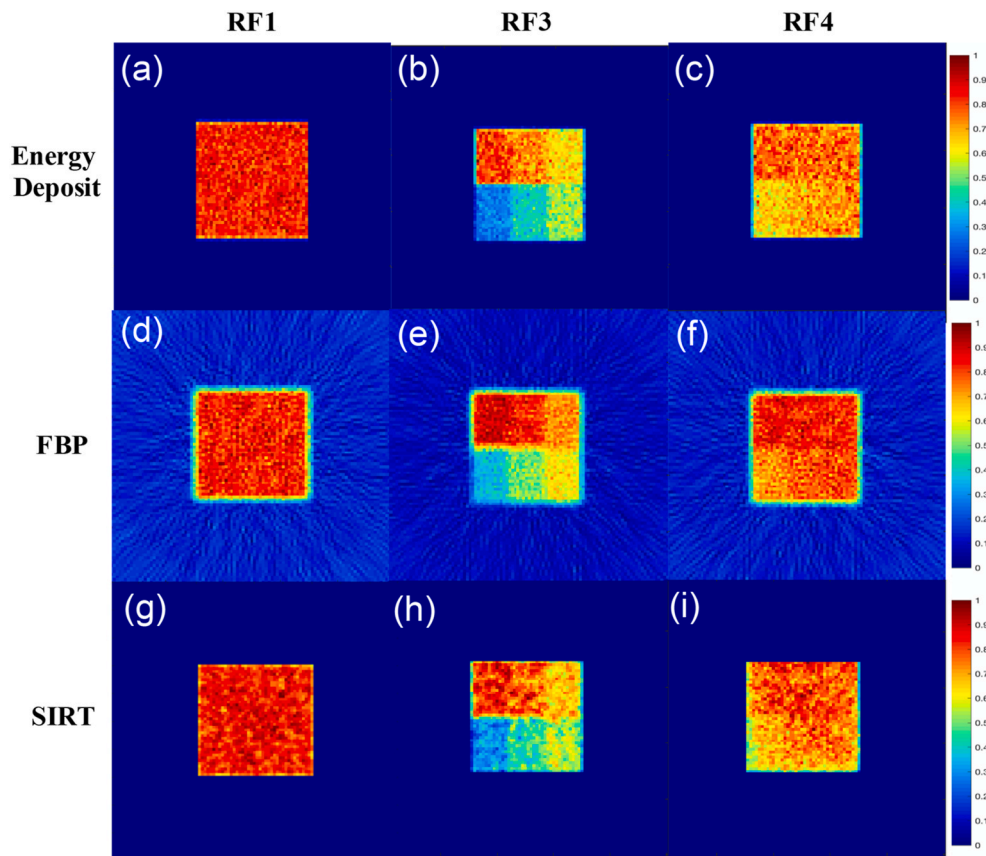
Fig. 10. Comparison of reconstruction effects between different reconstruction algorithms: (a–c) reference dose distribution; (d–f) dose distribution reconstructed by FBP algorithm; and (g–i) dose distribution reconstructed by SIRT algorithm.

Table 3
Quantitative comparison of reconstruction effects of different reconstruction algorithms.

Algorithm	Radiation field[a]	PSNR	SSIM	RMSE	VIF
FBP	RF1	15.045	0.070	0.177	0.503
	RF3	16.566	0.089	0.148	0.648
	RF4	15.275	0.075	0.172	0.595
SIRT	RF1	28.786	0.906	0.036	0.826
	RF3	28.964	0.916	0.036	1.023
	RF4	18.125	0.828	0.787	0.570

[a] RF1, square uniform radiation field; RF3, square uneven radiation field, flux ratio 10–50%; RF4, square uneven radiation field, flux ratio 1–8%.

3.6. Influence of rotation step size on dose reconstruction accuracy

The effect of different rotation step size on the reconstruction of the dose distribution is shown in Table 4. Due to its better reconstruction performance, SIRT is selected in the reconstruction algorithm. The image evaluation factors of the three different fields show that as the rotation step size increases the values of PSNR and VIF will decrease, while SSIM and RMSE each fluctuate around a value.

3.7. Influence of different radiation types on dose measurement accuracy

Figs. 6 and 12 show the results of dose distribution reconstruction under irradiation of 6 MV photons and 9 MeV electrons. According to the difference between the reference dose distribution and the target dose distribution, under photon irradiation, the difference in the center of the dose field is within 8% while the difference at the edge of the dose field is about 10%. The result for electrons has the same trend as for photons, but the difference is more distinct than photons in value.

In terms of image evaluation factors, under electronic irradiation, PSNR is 26.234, SSIM is 0.937, and RMSE is 0.049, indicating that the reconstructed dose distribution under two different radiation types has close results in image signal-to-noise ratio, structure, brightness, and contrast. However, in the information fidelity, VIF result of electron irradiation is 0.854 which is worse than that of photons.

3.8. IMRT dose field measurement

A beamlet of the prostate planning case (Bogner et al., 2009) is used to irradiate the optical fiber array to explore dose detection accuracy. Projection data at each angle, which is set as 3° per step, is shown in Fig. 13a; and dose deposit of the beamlet in the fiber array is shown in Fig. 13b. Reconstructed dose distribution in the two algorithms is shown in Fig. 13c and d. In the FBP algorithm, PSNR is 21.699, SSIM is 0.158, RMSE is 0.082, and VIF is 0.561; the difference to the reference dose is 5%. In the SIRT algorithm, PSNR is 24.943, SSIM is 0.935, RMSE is 0.057, and VIF is 0.780; the maximum difference between reference dose distribution and reconstructed dose distribution is 8%.

4. Discussion

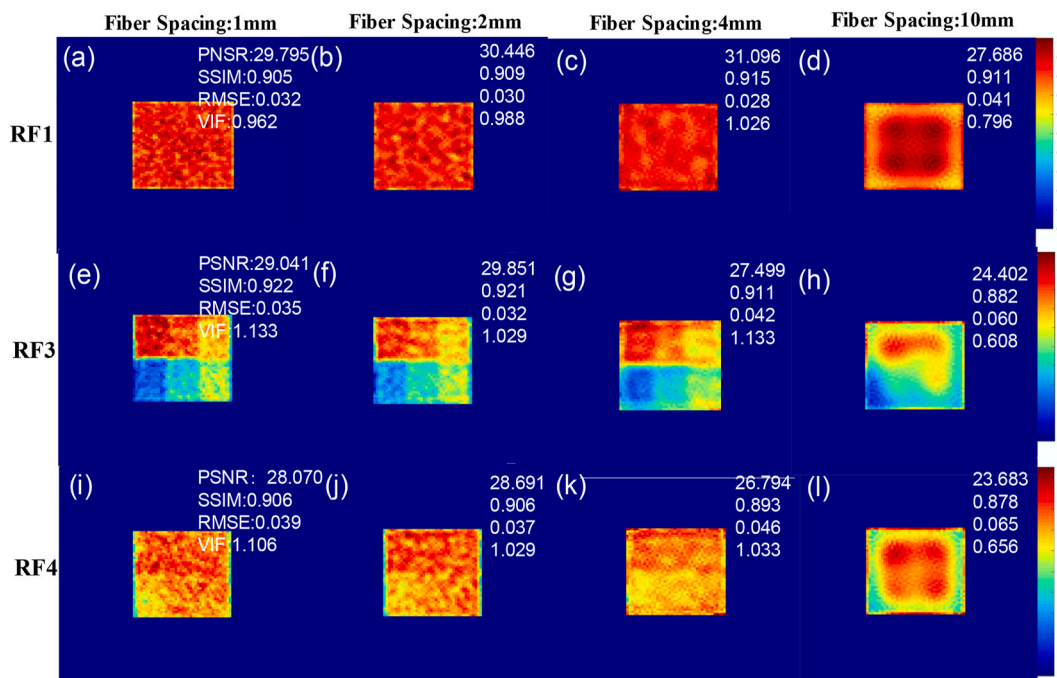Due to the unique advantages of optical fiber in the field of radiation

Fig. 11. Comparing the reconstruction accuracy among different fiber spacings: (a–d) dose field reconstruction with square uniform radiation field fiber spacing of 1, 2, 4, and 10 mm; (e–h) dose field reconstruction with square uneven (50%) radiation field fiber spacing of 1, 2, 4, and 10 mm; and (i–l) dose field reconstruction with a square uneven (8%) radiation field fiber spacing of 1, 2, 4, and 10 mm.

Table 4
Quantitative comparison of reconstruction effects with different rotation steps.

Radiation field[a]	Rotate step	PSNR	SSIM	RMSE	VIF
RF1	3	29.795	0.905	0.032	0.962
	6	28.786	0.906	0.036	0.826
	12	28.514	0.907	0.033	0.858
RF3	3	29.041	0.922	0.035	1.133
	6	28.964	0.916	0.036	1.023
	12	28.357	0.916	0.034	0.928
RF4	3	28.070	0.906	0.039	1.106
	6	27.177	0.895	0.044	0.944
	12	27.249	0.902	0.039	0.952

[a] RF1, square uniform radiation field; RF3, square uneven radiation field, flux ratio 10–50%; RF4, square uneven radiation field, flux ratio 1–8%.

detection, the optical fiber dosimeter is a promising tool for dose monitoring and measurement. Benefiting from previous research (Goulet et al., 2012; Son et al., 2015), we proposed an alternative 2D dose distribution monitoring method based on a rotating fiber array.

The results show that this method can well reconstruct the distribution of the dose in different shapes using the SIRT reconstruction algorithm. Using the SIRT reconstruction algorithm will have a better reconstruction accuracy but will also take longer, whereas using the FBP algorithm can quickly reconstruct the dose field but the reconstruction effect is less satisfactory due to streak artifacts. The above results are obtained for the rotation step of 3°. Therefore, the choice of reconstruction algorithm depends on the actual requirements for dose field reconstruction. The research results of Anam et al. (2019) show that when the number of iterations of SIRT exceeds 45, it will produce images with better spatial resolution and lower noise than FBP, which is consistent with the conclusions of our paper.

Fiber spacing is a parameter directly related to the resolution of the dose distribution reconstruction. As fiber spacing decreases, the projection information collected at each angle will increase, accuracy of the dose field reconstruction will increase, and the complexity and calculation of the system time will increase accordingly. When the fiber spacing is 2 mm, the reconstruction quality does not significantly decrease, and the calculation time is also shortened, which is the most efficient choice for reconstruction. The above results are obtained for a rotation step of 3°. If we sacrifice measurement time to reduce the rotation step, the reconstruction result should be better.

In dose field reconstruction, as the rotation step increases, the monitor time will decrease but it will also lead to a lack of information. Therefore, the SIRT algorithm is recommended. An appealing advantage of the SIRT is that it can use incomplete angle projection data to reconstruct the image. As the rotation step size increases, PSNR and VIF decrease meaning that the noise of the image increases and the accuracy of reconstructed dose distribution decreases. Therefore, 3° is recommended as the maximum rotation step, that is, at least 60 angles of projection data must be obtained for each rotation of 180°. This is also consistent with proposals of other researchers (Thaler et al., 2018; Z. Zhang et al., 2018). When they used deep learning methods to reconstruct sparse data CT images, in order to ensure high reconstruction accuracy, they also proposed that 60 angles of projection data is indispensable.

Under two different radiation types, this method can complete the function of 2D dose distribution reconstruction. The reconstruction accuracy for photons is better than for electrons for two main possible reasons: (1) electrons can be scattered easily so that Cherenkov photons can also be generated in the unirradiated area thus disturbing the reconstruction results; and (2) the Cherenkov photons generated by the fiber under electron irradiation have a strong angular dependence, that is, the number of Cherenkov photons produced by electrons at different angles is different (Lee et al., 2007). Due to the lack of electrons at some
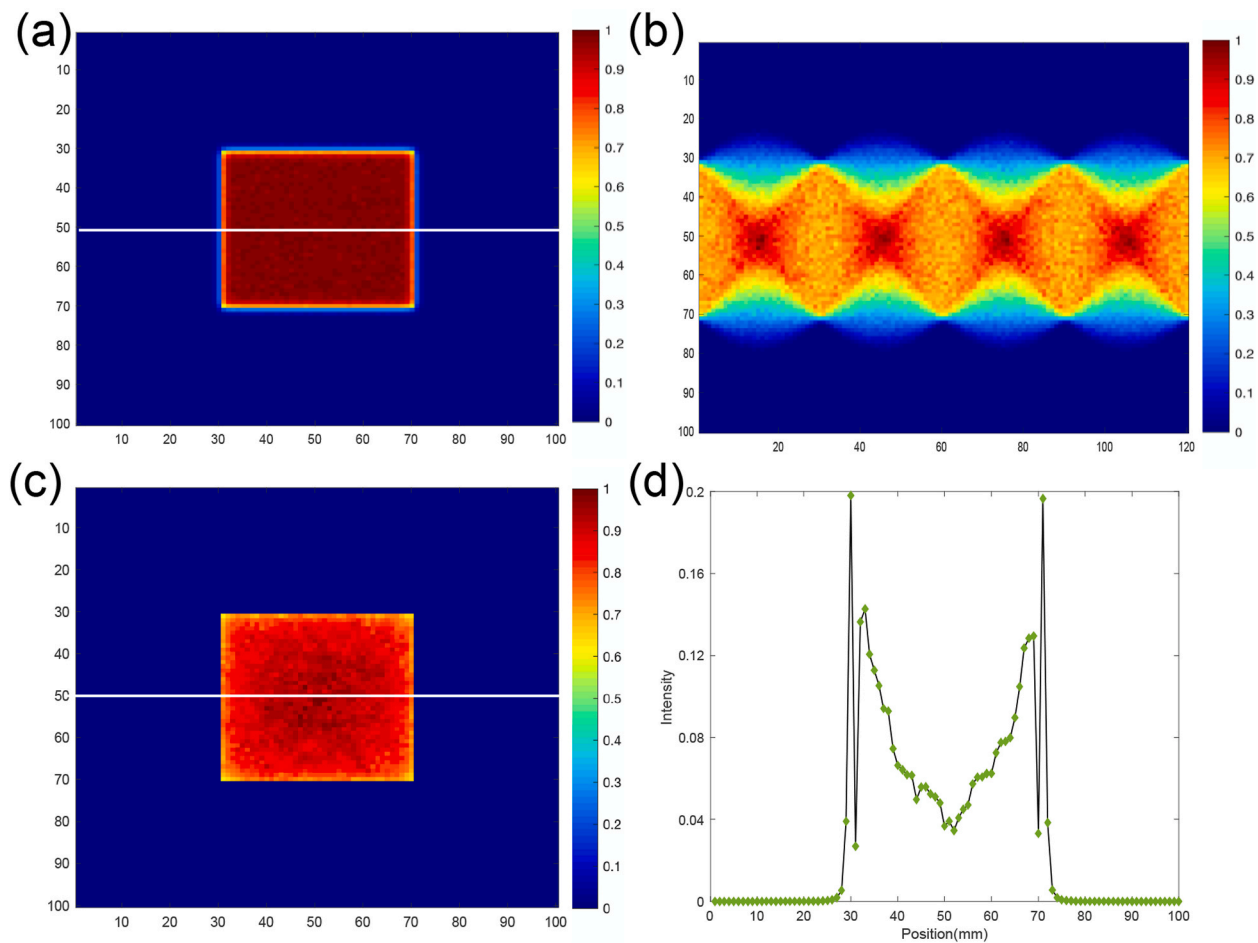
Fig. 12. Reconstruction accuracy comparison of RF1 under electron irradiation: (a) reference dose distribution of RF1; (b) sinogram of projection data; (c) reconstructed dose distribution of RF1; and (d) difference between reference dose distribution and reconstructed dose distribution.

incident angles, the fiber at the edge of the field generates less Cherenkov photons than the fiber at the center of the field, resulting in poorer accuracy of the reconstructed dose distribution compared to photons.

Although our method achieves 2D dose measurement, there are some limitations. That is, the dose difference is about 8–10%, which is not a satisfactory result. There are two main reasons. First, insufficient number of irradiated particles is the main reason for the error in the results. In clinical radiotherapy, the order of magnitude of emitted photons is about 10^{10}–10^{11} or even higher, while in the simulation the order of magnitude of emitted photons is lower. Because this Monte Carlo simulation includes interaction between radiation and material and optical transmission it makes it very time consuming. If we use the same order of magnitude as the clinical treatment, the calculation will take months or even years to obtain projection data of a radiation field, which is clearly unacceptable. Second, only some traditional reconstruction algorithms are used to reconstruct the 2D dose field. Recently, some novel image reconstruction methods that have a precise dose field reduction effect under different conditions have been proposed (Thaler et al., 2018; Z. Zhang et al., 2018). Additionally, electron contamination is not taken into account in setting of the photon energy spectrum. Also, this method needs to rotate 180° under irradiation to achieve reconstruction of the dose field distribution. Therefore, this is a static dose measurement method and cannot achieve real-time dose measurement. In actual experiments, we will also adopt new reconstruction algorithms, such as deep learning, to ensure that the difference in the reconstructed dose field in actual detection will not exceed 10%.

In the future, the rotating optical fiber array experimental platform could be used to reconstruct 2D dose field distribution under the irradiation of clinical linear accelerators. In following experiments, the rotating optical fiber array experimental platform will be placed free in air and some equivalent water placed above it considering the buildup effect. Pre-experiments based on this method have been carried out already. However, to implement the method in clinic, it may not be as limited as above applications, and more detailed research on clinical translation will be performed in following studies. We hope this platform can be used both in pretreatment QA and on-line QA.

5. Conclusion

In conclusion, this paper describes a 2D dose distribution monitoring method based on a rotating fiber array as an alternative pretreatment QA method. Based on the principle of CT, it can achieve static 2D dose measurement. Selecting the corresponding reconstruction algorithm, fiber spacing, and rotation angle according to different requirements when building a rotating fiber platform can maximize the reconstruction efficiency. The proposed method has the potential to achieve the acquisition of dose distribution information for pretreatment QA with relatively high spatial resolution and reusability.

Declaration of competing interest

The authors declare that they have no known competing financial interests or personal relationships that could have appeared to influence the work reported in this paper.
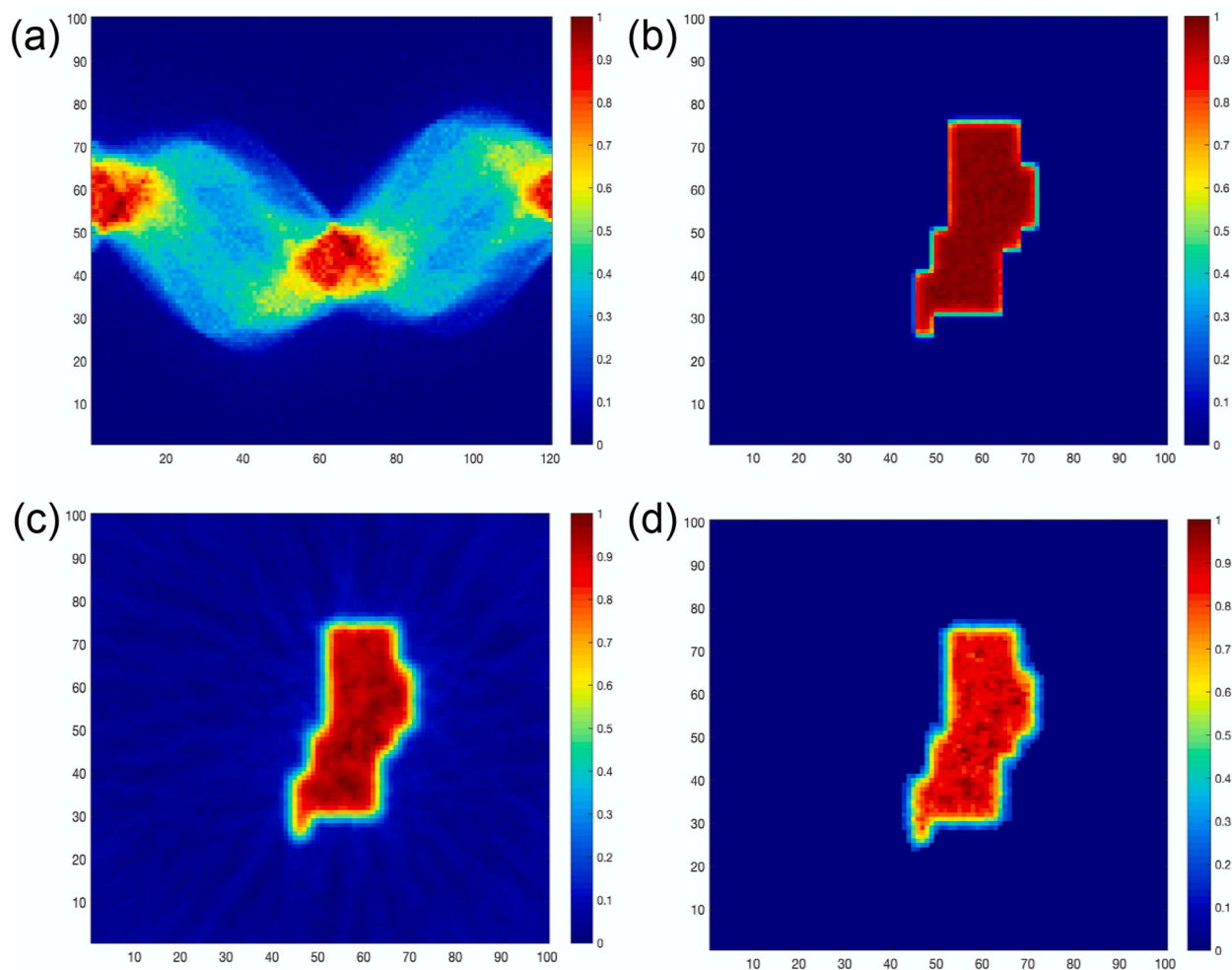
Fig. 13. Dose distribution reconstruction of IMRT beamlet: (a) sinogram of projection data; (b) reference dose distribution of IMRT beamlet; (c) reconstructed dose distribution of IMRT beamlet using FBP(Hann) algorithm; and (d) reconstructed dose distribution of IMRT beamlet using SIRT algorithm.

Acknowledgements

References

Agostinelli, S., Allison, J., Amako, K., Apostolakis, J., 2003. GEANT4 - a simulation toolkit. Nucl. Instruments Methods Phys. Res. Sect. A Accel. Spectrometers, Detect. Assoc. Equip. 506, 250–303. https://doi.org/10.1016/S0168-9002(03)01368-8.

Allison, J., Amako, K., Apostolakis, J., Araujo, H., Dubois, P.A., Asai, M., Barrand, G., Capra, R., Chauvie, S., Chytracek, R., et al., 2006. GEANT4 developments andapplications. IEEE Trans. Nucl. Sci. 53, 270–278. https://doi.org/10.1109/TNS.2006.869826.

Anam, C., Haryanto, F., Widita, R., Arif, I., Dougherty, G., 2019. An investigation of spatial resolution and noise in reconstructed CT images using iterative reconstruction (IR) and filtered back-projection (FBP). J. Phys. Conf. Ser. 1127 https://doi.org/10.1088/1742-6596/1127/1/012016.

Anchordoquia, L.A., McCauley, T.P., Paul, T., Reucroft, S., Swain, J.D., Taylor, L., 2001. Simulation of water Cerenkov detectors using GEANT4. Nucl. Phys. B 97, 2.

Archambault, L., Beddar, A.S., Gingras, L., Lacroix, F., Roy, R., Beaulieu, L., 2007. Water-equivalent dosimeter array for small-field external beam radiotherapy. Med. Phys. 34, 1583–1592. https://doi.org/10.1118/1.2719363.

Beaulieu, L., Beddar, S., 2016. Review of plastic and liquid scintillation dosimetry for photon, electron, and proton therapy. Phys. Med. Biol. 61, R305.

Bogner, L., Alt, M., Dirscherl, T., Morgenstern, I., Latscha, C., Rickhey, M., 2009. Fast direct Monte Carlo optimization using the inverse kernel approach. Phys. Med. Biol. 54, 4051–4067. https://doi.org/10.1088/0031-9155/54/13/007.

Brunner, S.E., Schaart, D.R., 2017. BGO as a hybrid scintillator/Cherenkov radiator for cost-effective time-of-flight PET. Phys. Med. Biol. 62, 4421–4439. https://doi.org/10.1088/1361-6560/aa6a49.

Caravaca, J., Descamps, F.B., Land, B.J., Wallig, J., Yeh, M., Orebi Gann, G.D., 2017. Experiment to demonstrate separation of Cherenkov and scintillation signals. Phys. Rev. C 95. https://doi.org/10.1103/PhysRevC.95.055801.

Cheng, Z.J., 2020. A Next-Generation Electronic Portal Imaging Device for Simultaneous Imaging and Dosimetry in Radiotherapy (PhD Thesis, University of Sydney).

Darafsheh, A., 2019. Fiber optic radioluminescent probes for radiation therapy dosimetry. Optical Fibers and Sensors for Medical Diagnostics and Treatment Applications XIX. International Society for Optics and Photonics, p. 108720Q.

Foster, R.D., Speiser, M.P., Solberg, T.D., 2014. Commissioning and verification of the collapsed cone convolution superposition algorithm for SBRT delivery using flattening filter-free beams. J. Appl. Clin. Med. Phys. 15, 39–49. https://doi.org/10.1120/jacmp.v15i2.4631.

Glaser, A.K., Zhang, R., Gladstone, D.J., Pogue, B.W., 2014. Optical dosimetry of radiotherapy beams using Cherenkov radiation: the relationship between light emission and dose. Phys. Med. Biol. 59, 3789.

Goulet, M., Archambault, L., Beaulieu, L., Gingras, L., 2013. 3D tomodosimetry using long scintillating fibers: a feasibility study. Med. Phys. 40, 101703. https://doi.org/10.1118/1.4819917.

Goulet, M., Gingras, L., Archambault, L., Beaulieu, L., 2012. High resolution 2D dose measurement device based on a few long scintillating fibers and tomographic reconstruction. Med. Phys. 38 https://doi.org/10.1118/1.3613015.

Izewska, J., Andreo, P., 2000. The IAEA/WHO TLD postal programme for radiotherapy hospitals. Radiother. Oncol. 54, 65–72. https://doi.org/10.1016/S0167-8140(99)00164-4.

Jenkins, C.H., Naczynski, D.J., Yu, S.J.S., Xing, L., 2015. Monitoring external beam radiotherapy using real-time beam visualization. Med. Phys. 42, 5–13. https://doi.org/10.1118/1.4901255.

Kalnins, C.A.G., Ebendorff-Heidepriem, H., Spooner, N.A., Monro, T.M., 2012. Radiation dosimetry using optically stimulated luminescence in fluoride phosphate optical fibres. Opt. Mater. Express 2, 62–70.

Kane, S.N., Mishra, A., Dutta, A.K., 2016. Preface: international conference on recent trends in physics (ICRTP 2016). J. Phys. Conf. Ser. 755, 8–12. https://doi.org/10.1088/1742-6596/755/1/011001.

Lee, B., Jang, K.W., Cho, D.H., Yoo, W.J., Shin, S.H., Kim, H.S., Yi, J.H., Kim, Sin, Cho, H., Park, B.G., Moon, J.H., Kim, Siyong, 2008. Measurement of two-dimensional photon beam distributions using a fiber-optic radiation sensor for small field radiation therapy. IEEE Trans. Nucl. Sci. 55, 2632–2636. https://doi.org/10.1109/TNS.2008.2002579.

Lee, B., Jang, K.W., Cho, D.H., Yoo, W.J., Tack, G.R., Chung, S.C., Kim, S., Cho, H., 2007. Measurements and elimination of Cherenkov light in fiber-optic scintillating detector for electron beam therapy dosimetry. Nucl. Instrum. Methods Phys. Res. 579, 344–348. https://doi.org/10.1016/j.nima.2007.04.074.

Markovic, M., Stathakis, S., Mavroidis, P., Jurkovic, I.A., Papanikolaou, N., 2014. Characterization of a two-dimensional liquid-filled ion chamber detector array used for verification of the treatments in radiotherapy. Med. Phys. 41 https://doi.org/10.1118/1.4870439.

Nascimento, L.F., Verellen, D., Goossens, J., Struelens, L., Vanhavere, F., Leblans, P., Akselrod, M., 2020. Two-dimensional real-time quality assurance dosimetry system using μ-Al$_2$O$_3$:C,Mg radioluminescence films. Phys. Imaging Radiat. Oncol. 16, 26–32. https://doi.org/10.1016/j.phro.2020.09.008.

O`Keeffe, S., McCarthy, D., Woulfe, P., Grattan, M.W.D., Hounsell, A.R., Sporea, D., Mihai, L., Vata, I., Leen, G., Lewis, E., 2015. A review of recent advances in optical fibre sensors for in vivo dosimetry during radiotherapy. Br. J. Radiol. 88 https://doi.org/10.1259/bjr.20140702.

Patil, B.J., Dhole, S.D., 2010. Studies on (i) characterization of bremsstrahlung spectra from high Z elements and (ii) development of neutron source using MEV pulsed electron beam and their applications. Proceedings, 55th DAE-BRNS Symposium on Nuclear Physics 55, 828.

Poobathy, D., Chezian, R.M., 2014. Edge detection operators: peak signal to noise ratio based comparison. Int. J. Image Graph. Signal Process. 6, 55–61. https://doi.org/10.5815/ijigsp.2014.10.07.

Rodríguez, C., López, A., García-Pinto, D., 2020. A new approach to radiochromic film dosimetry based on non-local means. Phys. Med. Biol. 65, 225019.

Sani, S.F.A., 2015. Characterisation of Defects and Thermoluminescence Yield of Novel Tailor-Made Doped Optical Fibres for Dosimetry. University of Surrey (United Kingdom).

Sheikh, H.R., Bovik, A.C., 2006. Image information and visual quality. IEEE Trans. Image Process. 15, 430–444. https://doi.org/10.1109/TIP.2005.859378.

Shu, D., Tang, X., Geng, C., Gong, C., Chen, D., 2015. Determination of the relationship between dose deposition and Cerenkov photons in homogeneous and heterogeneous phantoms during radiotherapy using Monte Carlo method. J. Radioanal. Nucl. Chem. 308, 187–193. https://doi.org/10.1007/s10967-015-4316-x.

Smith, R.L., Taylor, M.L., McDermott, L.N., Haworth, A., Millar, J.L., Franich, R.D., 2013. Source position verification and dosimetry in HDR brachytherapy using an EPID. Med. Phys. 40, 1–12. https://doi.org/10.1118/1.4823758.

Son, J., Kim, M., Shin, D., Hwang, U., Lee, S., Lim, Y., Park, J., Cho, K., Kim, D., Won, K., Yoon, M., 2015. Development of a novel proton dosimetry system using an array of fiber-optic Cerenkov radiation sensors. Radiother. Oncol. https://doi.org/10.1016/j.radonc.2015.07.045.

Thaler, F., Hammernik, K., Christian Payer, C., Urschler, M., Stern, D., 2018. Sparse-View CT Reconstruction Using Wasserstein GANs. In: International Workshop on Machine Learning for Medical Image Reconstruction. https://doi.org/10.1007/978-3-030-00129-2.

Tomashuk, A.L., Grekov, M.V., Vasiliev, S.A., Svetukhin, V.V., 2014. Fiber-optic dosimeter based on radiation-induced attenuation in P-doped fiber: suppression of post-irradiation fading by using two working wavelengths in visible range. Optic Express 22, 16778–16783.

Torres-Xirau, I., Olaciregui-Ruiz, I., Baldvinsson, G., Mijnheer, B.J., van der Heide, U.A., Mans, A., 2017. Characterization of the a-si EPID in the unity Mr-linac for dosimetric applications. Phys. Med. Biol. 63, 025006.

Villnow, M., Bosselmann, T., Willsch, M., Kaiser, J., 2014. FBG system for temperature monitoring under electromagnetic immersed and harsh oil and gas reservoir environment. Int. Conf. Opt. Fibre Sensors 9157, 915797. https://doi.org/10.1117/12.2059296.

Wang, Z., Bovik, A.C., Sheikh, H.R., Simoncelli, E.P., 2004. Image quality assessment: from error visibility to structural similarity. IEEE Trans. Image Process. 13, 600–612. https://doi.org/10.1109/TIP.2003.819861.

Widodo, P., Pawiro, S.A., Susila, I.P., 2020. Dosimetry for Intensity Modulated Radiotherapy (IMRT) Technique Using Ion Chamber Matrix (MatriXX-FFF) with Back Projection Method (Usual 6MV and 10MV), p. 12015. Journal of Physics: Conference Series. IOP Publishing.

Wong, J.H.D., Fuduli, I., Carolan, M., Petasecca, M., Lerch, M.L.F., Perevertaylo, V.L., Metcalfe, P., Rosenfeld, A.B., 2012. Characterization of a novel two dimensional diode array the magic plate as a radiation detector for radiation therapy treatment. Med. Phys. 39, 2544–2558. https://doi.org/10.1118/1.3700234.

Yang, Y., Ma, Y., Wang, Y., Dai, X., 2020. A rapid screening method for 32 P in urine samples by TDCR Cerenkov measurement. J. Radioanal. Nucl. Chem. 326, 369–377.

Zhang, X., Tang, X., Shu, D., Gong, C., Geng, C., Ai, Y., Yu, H., Shao, W., 2018. Theoretical calculation and measurement accuracy of Cerenkov optic-fiber dosimeter under electron and photon radiation therapies. Radiat. Meas. 110, 1–6. https://doi.org/10.1016/j.radmeas.2018.01.001.

Zhang, Z., Liang, X., Dong, X., Xie, Y., Cao, G., 2018. A sparse-view CT reconstruction method based on combination of DenseNet and deconvolution. IEEE Trans. Med. Imag. 37, 1407–1417. https://doi.org/10.1109/TMI.2018.2823338.